



Published in Image Processing On Line on 2018-11-23.  
Submitted on 2012-10-10, accepted on 2018-10-30.  
ISSN 2105-1232 © 2018 IPOL & the authors CC-BY-NC-SA  
This article is available online with supplementary materials,  
software, datasets and online demo at  
<https://doi.org/10.5201/ipol.2018.47>

# Study of the Principal Component Analysis Method for the Correction of Images Degraded by Turbulence

Tristan Dagobert<sup>1</sup>, Yohann Tendo<sup>2</sup>, Stéphane Landeau<sup>3</sup>

<sup>1</sup> CMLA, ENS Cachan, France ([tristan.dagobert@cmla.ens-cachan.fr](mailto:tristan.dagobert@cmla.ens-cachan.fr))

<sup>2</sup> UCLA Math Dept., Los Angeles, United States ([tendero@math.ucla.edu](mailto:tendero@math.ucla.edu))

<sup>3</sup> DGA, France ([stephane.landeau@intradef.gouv.fr](mailto:stephane.landeau@intradef.gouv.fr))

*Communicated by* Enric Meinhardt-Llopis

*Demo edited by* Tristan Dagobert

## Abstract

This article analyzes and discusses a well-known paper [D. Li, R.M. Mersereau and S. Simske, IEEE Letters on Geoscience and Remote Sensing, 3:4 (2007), pp. 340–344] that applies principal component analysis in order to restore image sequences degraded by atmospheric turbulence. We propose a variant of this method and its ANSI C implementation. The proposed variant applies to image sequences acquired with short as well as long exposure times. Examples of restored images using sequences of real atmospheric turbulence are presented. The acquisition of a dataset of image sequences with real atmospheric turbulence is described and the dataset is made available for download.

## Source Code

The ANSI C implementation of the source code, the code documentation, and the online demo are accessible at the [web page of this article](#)<sup>1</sup>.

## Supplementary Material

The image sequences used in this publication are available for download at the [web page of the article](#).

**Keywords:** turbulence; principal component analysis; image restoration; sharpening; real image sequences dataset

<sup>1</sup><https://doi.org/10.5201/ipol.2018.47>

# 1 Introduction

Atmospheric turbulence induces troublesome effects on the image formation of an optical instrument for long-range imaging. These effects result from the propagation of light through a turbulent medium, whose structural characteristics and evolution have been described by Kolmogorov [5]. Tatarski developed a theoretical model of the propagation of the light wave in this medium [10]. The image degradation phenomena associated with the imaging optical system were modeled by Fried [2] depending on the characteristics of the instrument, including the exposure time, the spatial resolution and the level of turbulence. Fried distinguishes between two classes of image degradation, depending on the exposure time used for image capture: the very long exposure and the very short exposure. From the perspective of the effects on the image, the short exposure ( $\ll 10$  ms) corresponds to an exposure time below which image degradation is not changing anymore. The degradation is thus not isoplanetic on the field of view. Some blur and spatial shift are randomly distributed in the image. An estimate of the average equivalent short exposure MTF (Modulation Transfer Function) is given by Fried [2]. A short exposure image taken at a later time ( $\gg 10$  ms) provides a totally different distribution of degradation. At long exposure capture, there is an accumulation of short exposure images taken at different times, which averages the non-isoplanetic effects. Degradation is then like a linear blur, similar to a convolution operator with a steady PSF (Point Spread Function), spatially and temporally. The long exposure MTF is estimated by Fried [2]. It appears from these analysis that the short exposure MTF provides, in general, according to the imaging configuration, a theoretical resolution substantially higher than the long exposure MTF, but at the cost of significant spatial distortion. To satisfy a criterion of sufficient image quality in short exposure imaging, it is necessary to correct these image defects. This can be achieved by two techniques. By optical correction of the light wavefront which aims to reverse, by optical methods applied in real time [1], the wavefront deformation induced by turbulence. By image processing, considering that the spatial and temporal variability of turbulence makes possible the probable finding of a resolution optimum in an image sequence, for every given locality; with the proviso that the observed scene is fixed. This is the principle of “lucky imaging” [3].

Most of the time, principal components analysis (PCA) is used in image processing as an intermediate step. PCA extracts an orthonormal basis adapted to the observed data. The basis vectors are usually sorted in order to obtain a decreasing variance of the data projected onto them. For example in the works of Liu et al. [9], the PCA is employed with optical flow in order to discriminate a moving vehicle from its moving environment. In the work of Turk et al. [11] the PCA permits to reduce the space of example images used during the learning stage of a recognition algorithm.

In [7] Li et al. propose to use PCA to restore turbulence degraded image sequences (see Figure 1). This paper proposes a variant of [7] and its implementation. We provide numerical results on real turbulence degraded image sequences. The sequences used for the experiments are made available for download.

The paper is divided in five sections. Section 2 provides the PCA formalism. Section 3 gives the numerical method of Li et al. as it is given in [7] and discusses it. Section 4 proposes a variant of the Li et al. method. Section 5 provides the details and implementation of the proposed numerical method. Section 6 gives experimental results obtained from real atmospheric turbulence. Appendix A describes the experimental protocol used to acquire the sequences used for the experiments. Appendix B gives a practical computation of the eigenvectors and Appendix C provides informations about the online demonstrator.

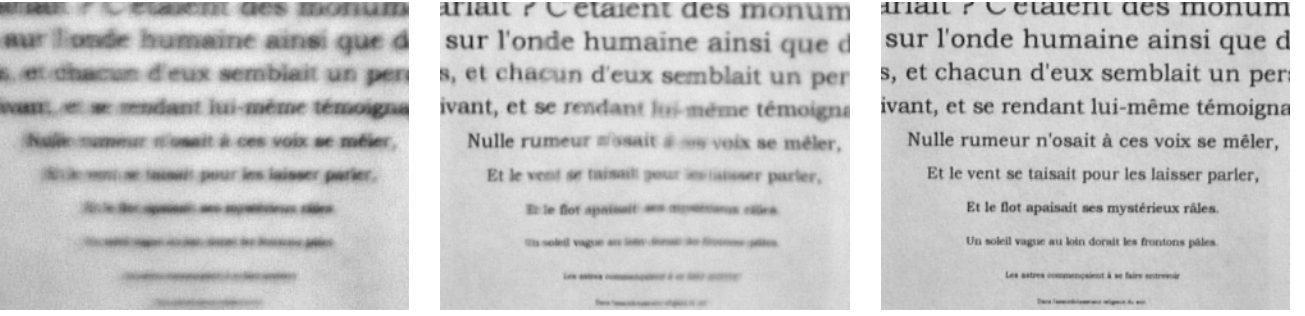


Figure 1: Examples of images deteriorated by atmospheric turbulence with a dominant blur on the left panel, dominant distortion in the middle and the ground truth on the right panel.

## 2 PCA Concept

Let  $\Phi$  be a dataset described by  $N$  parameters subject to  $M$  observations  $\Phi_m \in \mathbb{R}^N$ . These observations  $\Phi_m$  are represented by  $M$  points in the parameters space  $\mathbb{R}^N$ . The PCA allows to reduce the number of parameters  $N$  to  $q \leq N$  with a linear transformation, while retaining as much of the “variability” of the observed data as possible. In other words, the PCA method consists in determining a sub-space of  $q \leq N$  dimensions which captures as much of the variance of the dataset as possible. Alternatively, the subspace found by the PCA method is the one that minimizes the projection error, measured as the sum of squared Euclidean norms between each point and its projection. For this purpose, a basis  $\mathbf{v}$  of vectors  $v_i \in \mathbb{R}^q$  is iteratively built. The first vector  $v_1$  is obtained by maximizing the following quantity

$$\sigma_{v_1}^2 = \frac{1}{M} \sum_{m=1}^M (\pi(\Phi_m - \mu))^T (\pi(\Phi_m - \mu)) = v_1^T \underbrace{\frac{1}{M} \left[ \sum_{m=1}^M (\Phi_m - \mu)(\Phi_m - \mu)^T \right]}_{\Sigma} v_1 = v_1^T \Sigma v_1, \quad (1)$$

where  $\mu = \frac{1}{M} \sum_{m=1}^M \Phi_m$  is the barycenter of the  $M$  observations  $\Phi_1, \dots, \Phi_M$ ,  $\pi(\Phi_m) = \langle \Phi_m, v_1 \rangle v_1$  the projection of  $\Phi_m$  upon  $v_1$ ,  $(\Phi_m - \mu)^T$  denotes the transpose of  $\Phi_m - \mu$  and  $\Sigma \in \mathcal{M}_{N \times N}(\mathbb{R})$  is the covariance matrix of the vectors  $\Phi_1, \dots, \Phi_M$ . Remark that the quantity  $\sigma_{v_1}^2$  in (1) is the variance of the observations projected on the vector  $v_1$ . The maximization of  $\sigma_{v_1}^2$  defined in (1) is an optimization problem that can be formulated by the Lagrangian equation

$$\mathcal{L} = v_1^T \Sigma v_1 + \lambda(1 - v_1^T v_1),$$

which extremum condition  $\partial_v \mathcal{L} = 0$  leads to the eigenvalues equation

$$\Sigma v_1 = \lambda v_1.$$

From a numerical point of view, the iterative building of the basis  $\mathbf{v}$  boils down to computing the  $q$  first eigenvectors related to the  $q$  greatest eigenvalues of the covariance matrix  $\Sigma$  defined in Equation (1).

## 3 The Method of Li et al.

In [7, 8] Li et al. propose to apply PCA to a sequence of  $M$  image frames  $(I_m)_{m \in \{1, \dots, M\}}$  degraded by atmospheric turbulence in order to produce one corrected image  $J$  ( $J$  is an estimation of an “ideal” image  $I$ ). This section studies the Li et al. method [7, 8]. Section 3.1 gives the numerical procedure as it is given in their publications [7, 8]. Section 3.2 discusses the numerical method proposed by Li et al. in [7, 8].

### 3.1 Description

In [7, 8] Li et al. consider each frame  $I_m$  of size  $N$  pixels rearranged in the form of column vectors so that  $I_m \in \mathbb{R}^N$ . Consequently, hereinafter we shall define the  $m$ -th image frame denoted  $I_m$  by

$$I_m : \begin{array}{l} \{0, \dots, N-1\} \\ j \end{array} \rightarrow [0, 1] \\ \qquad \qquad \qquad \qquad \qquad \mapsto I_m(j).$$

This discrete image frame  $I_m$  has pixel values in the interval  $[0, 1]$  and is considered to be a degraded version of a crisp image  $I$ . Here and in the sequel, we shall denote by  $(I_m)_{m \in \{1, \dots, M\}}$  a sequence of  $M$  degraded images that we observe. The goal of the Li et al. method is to estimate the crisp image  $I$  given the observed image sequence  $(I_m)$ .

With the above conventions,  $I_m$  corresponds to  $\Phi_m$  of Section 2. Indeed, each image frame  $I_m \in \mathbb{R}^N$  is one of the  $M$  observations. In addition, the  $N$  pixel values of each frame  $I_m$  are the measurement parameters.

In [7, 8] the authors assume that the degradation model is given by a convolution, i.e., formally

$$I_m := h_m * I \text{ (see [7, equation 2, page 2])}, \quad (2)$$

where each  $h_m$  is an unknown convolution kernel at time  $m \in \{1, \dots, M\}$  and  $*$  denotes the standard discrete convolution. The convolution kernels  $h_m$  are assumed to be low-pass filters. In [7] Li et al. provide an intuitive explanation on how the PCA can restore turbulence degraded images that we quote extensively [7, page 1]:

“The first principal component can be used as such an estimate since it has maximum variance and it contributes most to the variance of the observed dataset. Intuitively, blurring is a smoothing process in which the high-frequency components are removed and the variance is reduced. Thus, deblurring should be able to boost high-frequency components to some extent to restore the image. Variance can be viewed as a measurement of high-frequency components in an image. Previously, we developed a constrained variance maximization method for blind image deconvolution [8]. That variance maximization is equivalent to a PCA.”

Li et al. seem to identify variance of a dataset of images (the one maximized by the subspace defined by PCA) with the high frequency content in an image, although these are different things. A priori there is no evident relation between these two things. However, as we show later, for a dataset generated by applying different amounts of blur to a given image, the principal component can indeed be related to the high frequencies of the image.

Having described the observation model proposed in [7] we are now in position to detail the numerical method as it is proposed [7, section II, pages 2-3].

The first step centers the input data  $(I_m)_{m \in \{1, \dots, M\}}$ . We recall that each  $I_m \in \mathbb{R}^N$  is an observed image frame degraded by turbulence. Thus, the temporal average  $\mu$  of the image sequence is computed

$$\mathbb{R}^N \ni \mu := \frac{1}{M} \sum_{m=1}^M I_m. \quad (3)$$

The observed data is then centered by subtracting the average image  $\mu$  as

$$\mathbb{R}^N \ni G_m := I_m - \mu \text{ for } m \in \{1, \dots, M\}.$$

The second step consists in computing the PCA. Therefore, the matrix  $A := [G_1 \dots G_M] \in \mathcal{M}_{N \times M}(\mathbb{R})$  is built by a straightforward concatenation of the  $G_m$  vectors. The covariance matrix

$\Sigma \in \mathcal{M}_{N \times N}(\mathbb{R})$  associated with  $A$  is  $\Sigma := \frac{1}{M}AA^T$ , where  $A^T$  denotes the transpose of the matrix  $A$ . A direct computation of eigenvalues and eigenvectors of  $\Sigma$  is not numerically tractable. Indeed,  $N$  is the number of pixels of the observed images and is therefore large.

To circumvent this issue, we notice that to compute the eigenvectors of  $\Sigma$  it suffices to calculate the eigenvectors  $v_i$  of the much smaller matrix  $A^T A \in \mathcal{M}_{M \times M}(\mathbb{R})$  where  $M \ll N$ . (A proof is given in Annex B.)

From the previous step, extract  $v_1$  the eigenvector of  $\Sigma$  associated to the eigenvalue of highest absolute value. The last step consists in computing the restored frame  $J$

$$J := \mu + Av_1 \quad [7, \text{equation 11 page 3}]. \quad (4)$$

Assuming that formula (4) makes sense, it is interpreted by Li et al. [7, 8] as follows. On the one hand, it is clear that the average image  $\mu$  contains temporal low frequencies of the image sequence. It is a rough estimate of the ideal underlying observed scene  $I$ . On the other hand,  $Av_1$  acts as a “filter to boost the high frequency content” [7, section II, page 3].

Note that the number  $M$  of frames used in reconstruction is specified in [7, 8] as nine frames. Having recalled the numerical method proposed by Li et al. as it is given in [7, 8] we are now in position to discuss it.

### 3.2 Discussion of the Method of Li et al.

The algorithm of Li et al. leads to three remarks.

First of all, formula (4) is not well defined. Indeed, an eigenvector is only defined up to a multiplicative constant. As a consequence:

1.  $\mu$  and  $Av_1$  can have arbitrarily different norms. Therefore, adding them as in Equation (4) requires a normalization so that they have compatible dynamics;
2.  $Av_1$  can also change direction (sign) depending on the numerical implementation of the method that extracts the eigenvector  $v_1$ . Therefore, adding  $Av_1$  to  $\mu$  without fixing the direction of the vector  $Av_1$  does not make sense.

This lack of definition is illustrated in Figure 2. In principle the numerical method proposed in [7] and described in Section 3.1 is invariant with respect to time indexes permutation. Indeed, neither the mean  $\mu$  nor the first PCA component  $Av_1$  that appears in (4) depends on the order of the observations. However, Figure 2 shows that for a fixed numerical implementation of the PCA the output depends on the order of the input frames. In the first case, ten inputs frames are used as input in the order acquired by the camera  $\mathcal{W}_1 = (I_1, I_2, I_3, \dots, I_8, I_9, I_{10})$ . In the second case two images are permuted so we have  $\mathcal{W}_2 = (I_8, I_2, I_3, \dots, I_1, I_9, I_{10})$ . (In practice, this permutation situation can occur due to the randomness of the turbulence.) The two obtained images differ, as illustrated on the right panel of Figure 2 and illustrates the fact that the Li et al. method [7, 8] is not correctly defined.

Lastly, in [7, 8] Li et al. the use of the single first principal component is justified by an intuitive reasoning that does not imply that the others components are useless. As a matter of fact, Figure 3 shows that the use of the second component can yield better results than the use of the first component.

We have reviewed the method proposed in [7]. The next section proposes a variant of the method proposed in [7] that solves the theoretical and practical issues raised in Section 3.2.



Figure 2: On the left panel the image produced using the image sequence  $\mathcal{W}_1 = (I_1, I_2, I_3, \dots, I_8, I_9, I_{10})$ . On the right the image produced using  $\mathcal{W}_2 = (I_8, I_2, I_3, \dots, I_1, I_9, I_{10})$  as input sequence. Both result differ. This is a direct consequence of mathematical indefiniteness of (4).

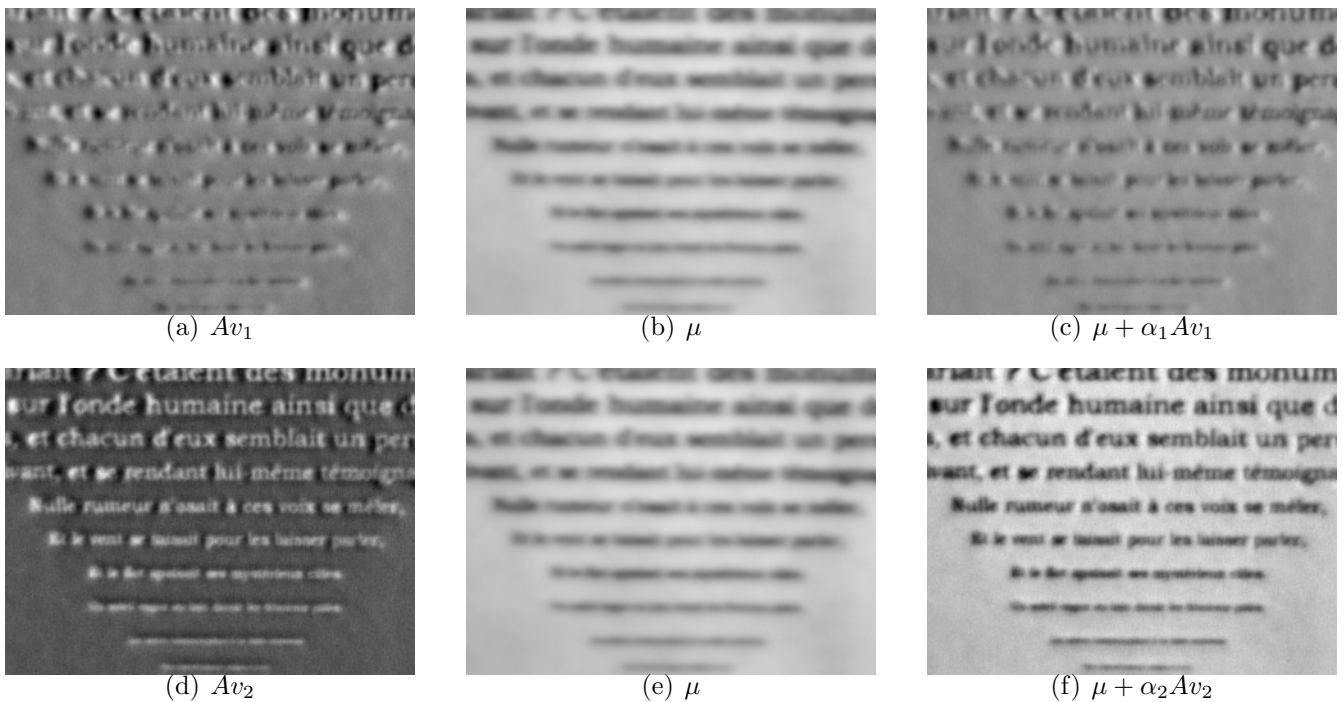


Figure 3: These figures show that the second component  $A_{v_2}$  can yield better results than the first component  $A_{v_1}$  on a real turbulence degraded image sequence. Indeed, the second component depicted in Figure 3(d) is much sharper than the first component depicted in Figure 3(a). Figures 3(b) and 3(e) depict the temporal average image  $\mu$ . Figure 3(c) (resp. 3(f)) depicts a possible result using the first component (resp. the second component). For these experiments, the values of  $\alpha_1$  and  $\alpha_2$  have been tuned manually.

## 4 Selected Principal Component Algorithm (SPCA)

As we have seen in Section 3.2, the Equation (4) that underlies the method proposed in [7, 8] is not well-defined. The goal of this section is to propose a variant of [7, 8] that circumvents this issue.

To cope with the fact that eigenvectors  $v_i$  are defined up to a sign and that  $Av_i$  can have arbitrary norms our first goal is to propose an adequate normalization. Therefore, we propose

1. to normalize the norms of the first component  $Av_i$  by  $w_i = \frac{Av_i}{\|Av_i\|}$ , where  $\|\cdot\|$  denotes the  $\ell_2$ -norm;
2. to normalize the directions by using the inner product  $\frac{\langle \Delta\mu, w_i \rangle}{|\langle \Delta\mu, w_i \rangle|}$  rather than  $w_i$  where  $\Delta\mu$  denotes the Laplacian of  $\mu$ .

Using these two modifications we can define the restored image  $J$  as

$$J = \mu - \epsilon \frac{\langle \Delta\mu, w_i \rangle}{|\langle \Delta\mu, w_i \rangle|} w_i, \quad (5)$$

where we assume that  $\langle \Delta\mu, w_i \rangle \neq 0$ . Index  $i$  allows us to select which component is used in the reconstruction and  $\epsilon > 0$  is a sharpening parameter.

We justify these modifications as follows. First, if we choose  $i = 1$  in Equation (5) we retrieve a well defined variant of Equation (4). Secondly, the vector  $\frac{\langle \Delta\mu, w_i \rangle}{|\langle \Delta\mu, w_i \rangle|} w_i$  has always the same direction as  $\Delta\mu$ . This means that (5) behaves similarly to an inverse heat equation and tends to sharpen the average image  $\mu$ .

**Principal component selection.** Our goal is to remove the blur caused by the turbulence. As we have seen in Section 3.2, Li et al.'s method has a natural interpretation in terms of inverse heat equation. Therefore, we propose to choose the (normalized) principal component  $w_i$  that maximizes  $|\langle \Delta\mu, w_i \rangle|$ . This means that we use the  $w_i$  that produces the most sharpening effect.

In principle, we should compute  $|\langle \Delta\mu, w_i \rangle|$  for every principal component  $w_i$ . However, experimentally it is enough to compute  $|\langle \Delta\mu, w_1 \rangle|$  and  $|\langle \Delta\mu, w_2 \rangle|$ . This fact is experimentally illustrated in Figure 4 that depicts the four first principal components on two examples. Experimentally, the components of order higher than 2 are very noisy.

### 4.1 Analysis of the Gaussian Convolution Model

We study the principal direction of a set of Gaussian blurred versions of an image. The sequence of turbulence degraded images is assumed to follow the convolution degradation model

$$I_m = h_m * I.$$

We will additionally assume that the low-pass filters  $h_m$  are Gaussian filters with different variances

$$h_m(x) = \frac{1}{2\pi\sigma_m^2} \exp\left(-\frac{|x|^2}{2\sigma_m^2}\right).$$

According to the results of Hufnagel and Stanley [4], this is a reasonable approximation for long exposures. In the following we will use the notation  $h_{\sigma_m} = h_m$ .

A first order Taylor approximation around  $\sigma_0$  for the filtered images  $I_m$  reads as follows

$$I_m = I * h_{\sigma_m} = I * h_{\sigma_0} + \frac{d}{d\sigma}(I * h_{\sigma})|_{\sigma_0}(\sigma_m - \sigma_0) + O((\sigma_m - \sigma_0)^2).$$

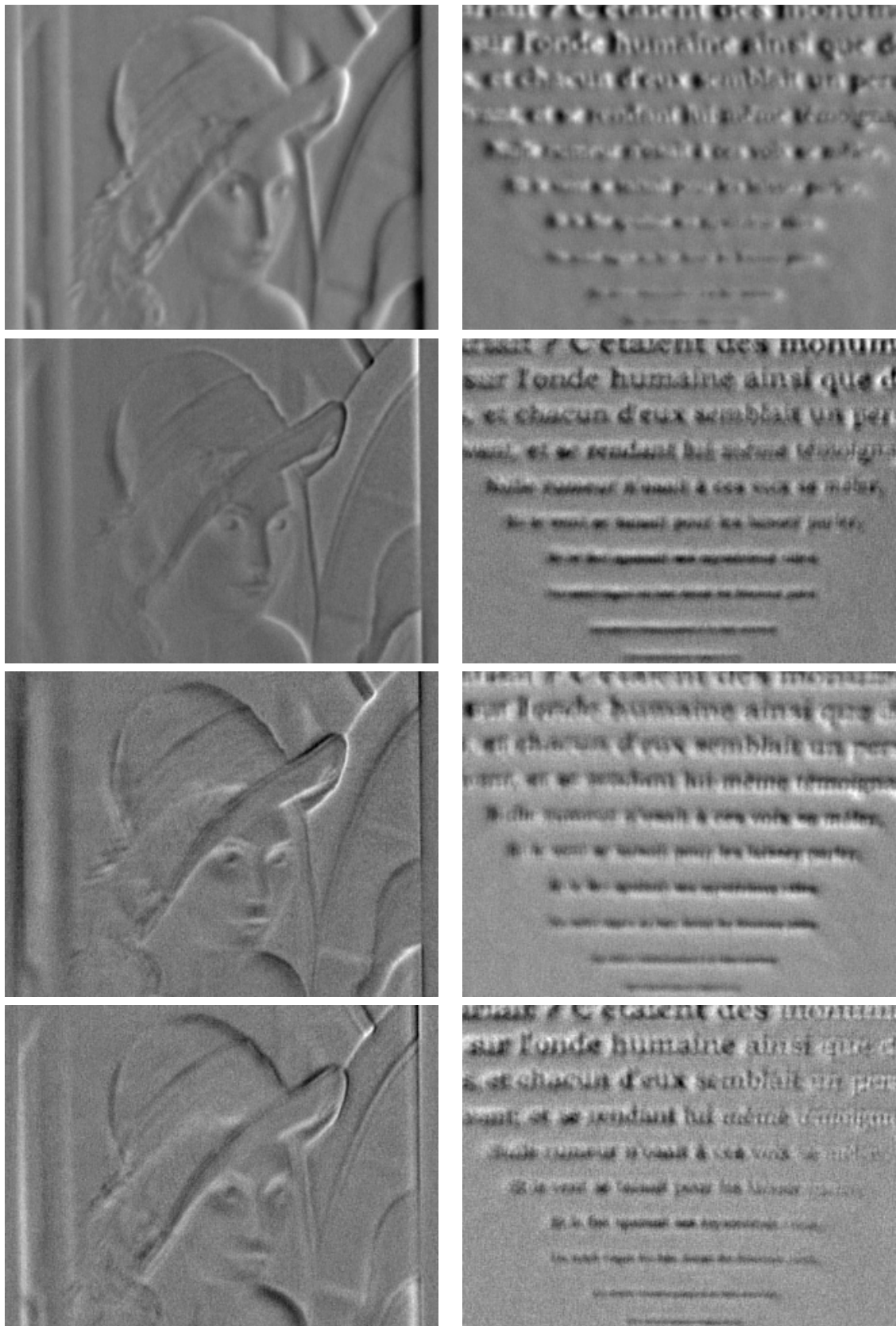


Figure 4: From top to bottom, the first four components of the PCA decomposition of Lena and the poem. The presence of noise is more apparent as the order of the components increase.

Due to the linearity of the convolution we have that  $\frac{d}{d\sigma}(I * h_\sigma) = I * \frac{d}{d\sigma}h_\sigma$ . For a Gaussian filter, we have that

$$\frac{d}{d\sigma}h_\sigma = -\frac{1}{\pi\sigma^3} \left(1 - \frac{|x|^2}{2\sigma^2}\right) \exp\left(-\frac{|x|^2}{2\sigma^2}\right) = \sigma\Delta h_\sigma.$$

Thus  $\frac{d}{d\sigma}(I * h_\sigma) = I * \sigma\Delta h_\sigma = \sigma\Delta(I * h_\sigma)$ , and we have that

$$I_m = I * h_{\sigma_0} + \sigma\Delta(I * h_{\sigma_0})(\sigma_m - \sigma_0) + O((\sigma_m - \sigma_0)^2). \quad (6)$$

According to this simple model, the family of turbulence degraded images describes a curve. The line tangent to the curve is given by the first two terms in the Taylor polynomial. If we assume that  $\delta\sigma$  is sufficiently small, we can neglect the second order error term, and approximate the curve by its tangent line at  $\sigma_0$ .

If we perform PCA on a set of images generated by drawing  $\sigma \sim \mathcal{U}([\sigma_0 - \delta\sigma, \sigma_0 + \delta\sigma])$ , for a sufficiently small  $\delta\sigma$ , we would get

$$\mu = \frac{1}{N} \sum_{m=1}^N I * h_m \approx I * h_{\sigma_0} \quad \text{and} \quad v_1 \propto \sigma\Delta(I * h_{\sigma_0}) = \sigma\Delta\mu,$$

where  $v_1$  is the first principal direction. The other principal direction should have negligible variance.

In summary, if the turbulence is modeled as a convolution with Gaussian low-pass filters with variances distributed around a given  $\sigma_0$ , then the first principal direction approximates  $\Delta\mu$ . Under this assumptions the ‘‘inverse heat equation’’ method is therefore closely related to the proposed method.

The approximation is good when all variances  $\sigma_m$  are close to a mean variance  $\sigma_0$ , and worsens as their spread increases. The reason is that the linear approximation to the curve  $I * h_\sigma$  is less valid. In this case, not only  $v_1$  is not aligned with  $\Delta\mu$ , but also the other principal directions become more important, due to the curvature of the set.

An advantage of the proposed method is that it is more robust to noise. If the acquired images are noisy, the mean  $\mu$  has still some noise, which is amplified severely by the Laplacian operator. On the other hand, the principal component  $v_1$  is less affected by noise.

## 5 Numerical Implementation

This section gives the implementation details of the SPCA method described in Section 4. Algorithm 1 provides the pseudo code that is implemented in the files `pca_method.c` and `ccmath.c`.

**Input/Output re-quantification.** The input images  $I_m$  are read in PNG 8-bit format ( $I_m$  takes values in  $\{0, \dots, 255\}$ ) and are re-quantized to have values in  $[0, 1]$  by dividing every pixel values by 255. We now justify this re-quantification.

Consider an image of size  $N = 640 \times 480 \approx 3 \cdot 10^5$ . On the one hand, if the pixel value is around  $2 \cdot 10^2$  then  $A^T A(i, j) = \sum_{n=1}^N A^T(i, n)A(n, j) \approx N(2 \cdot 10^2)^2 \approx 7 \cdot 10^9$ . This very large values lead to numerical issues when calculating eigenvalues (step 1 of Algorithm 1) because of the lack of single point precision. On the other hand, if the pixel value is  $\frac{2 \cdot 10^2}{255}$  then  $A^T A(i, j) \approx 2 \cdot 10^5$  which is enough to solve the numerical issue.

This re-quantification is inverted in step 4 of Algorithm 1. To be precise, the pixel values of the output images are point-wise multiplied by 255.

**Algorithm 1:** The Selected Principal Component Algorithm (SPCA).

---

**input** :  $M$  image frames  $I_m$ ,  $m \in \{1, \dots, M\}$   
**input** :  $\epsilon > 0$  sharpening parameter  
**output**:  $J$  the corrected image  
**output**:  $\mu$  the temporal mean image  
**output**:  $L$  the Laplacian subtraction comparison image, optional

Compute the temporal mean image  $\mu := \frac{1}{M} \sum_{m=1}^M I_m$   
**for**  $m \leftarrow 1$  **to**  $M$  **do**  
    $G_m \leftarrow I_m - \mu$   
 build matrix  $A \leftarrow [G_1 \dots G_M]$

- 1 compute the  $M$  eigenvalues and eigenvectors  $(\lambda_i, v_i)$  of  $A^T A$   
 sort the eigenvectors  $v_i$  according to the decreasing order of  $|\lambda_i|$
- 2 compute the orthonormal vectors  $w_i \leftarrow Av_i / \|Av_i\|$
- 3 compute  $\Delta\mu$ , the Laplacian of  $\mu$   
 select  $w_a \leftarrow \arg \max_{w_i} |\langle \Delta\mu, w_i \rangle|$  with  $i \in \{1, 2\}$   
**if**  $\langle \Delta\mu, w_a \rangle > 0$  **then**  
    $w_b \leftarrow +w_a$   
**else**  
    $w_b \leftarrow -w_a$   
 $J \leftarrow \mu - \epsilon \cdot w_b$
- 4 record  $J$
- 5 **optionally**  $L \leftarrow \mu - \epsilon \cdot \Delta\mu / \|\Delta\mu\|$  (classical inverse heat equation)
- 6 **optionally** record  $L, \mu$

---

**Step 1 (Computation of the principal components).** The determination of eigenvalues and eigenvectors is carried out by using a three-step general algorithm for singular value decomposition:

1. Householder transforms, starting with  $A^T A$ , in order to compute  $U_1$ ,  $V_1$  and  $F$  so that  $A^T A = U_1 F V_1^T$ , where  $U_1$  and  $V_1$  are orthogonal matrices and  $F$  is a bidiagonal matrix;
2. matrix reduction of type  $QR$  starting with  $F$  so that  $F = U_2 D V_2^T$  where  $D$  is the eigenvalues matrix of  $A^T A$ ;
3. recomposition of  $A^T A = U F V^T = U_1 (U_2 D V_2^T) V_1^T = (U_1 U_2) D (V_1 V_2)^T$  where  $U = U_1 U_2$  (resp.  $V^T = (V_1 V_2)^T$ ) is the eigenvectors matrix (resp. transpose) of  $A^T A$ .

The functions used to calculate these quantities are part of the C library “Ccmath”.

**Step 2 (Computation of  $w_m$ ).** As vectors  $G_i$  are centered around  $\mu$  they are not linearly independent and belong to a hyperplane of dimension  $M - 1$ . So the  $M^{\text{th}}$  vector no longer belongs to this hyperplane (explanation specified in [6] paragraph 1.3.7). So we do not consider vector  $v_M$  in the composition of  $J$ . More specifically, the computation  $w_M := \frac{Av_M}{\|Av_M\|}$  can cause infinite or non-numeric values. Therefore  $v_M$  is set to zero.

**Step 3 (Computation of  $\Delta\mu$  the Laplacian of  $\mu$ ).** The Laplacian filter is defined as the  $3 \times 3$  discrete filter, explicitly given in (7)

$$\mathcal{L} = \begin{bmatrix} 1 & 1 & 1 \\ 1 & -8 & 1 \\ 1 & 1 & 1 \end{bmatrix}. \quad (7)$$

The Laplacian of  $\mu$  is computed by a discrete convolution (with periodic boundaries conditions) of  $\mu$  and  $\mathcal{L}$ .

**Step 5.** To compare the effects of the proposed SCPA filter with the Laplacian filter on a given image and a similar filter coefficient  $\epsilon$ , these filters should have the same order of magnitude. On the one hand, the vectors of the SPCA are normalized with zero mean and their variance is  $\frac{1}{N}$  (according to the König-Huyghens theorem). On the other hand, the Laplacian is zero mean and it suffices to normalize the vector  $\Delta\mu$  by its  $\ell^2$  norm to retrieve the same variance. Thus, the time step of the inverse heat equation is compatible with the parameter of the SPCA algorithm and conducts to the relation

$$L = \mu - \epsilon \frac{\Delta\mu}{\|\Delta\mu\|}. \quad (8)$$

## 6 Examples and Experiments

We conducted two experiments using three sets of sequences marked A, B and C. Dataset A contains images as they were acquired by the camera; it is composed of six real image sequences distorted and blurred by atmospheric turbulence. Appendix A details the acquisition protocol. Each sequence contains 200 images. Dataset B (resp. C) consists of images of A which were averaged on 20 (resp. 10) frames so that each sequence contains 10 (resp. 20) images. The first experiment was to study the behavior of SCPA with respect to the Laplacian filter in the case of sequences acquired using short exposure time. The second experiment was to get closer to the assumptions of Li et al. [8] by considering a long exposure time and to observe the influence of the SCPA filter when varying  $M$  and the exposure time. We performed measurements of PSNR and MSSIM in these experiments. The PSNR is defined by

$$PSNR(J, I_r) = -10 \log_{10}(MSE(J, I_r)/Q^2),$$

where

$$MSE(J, I_r) = \frac{1}{N} \sum_{k=0}^{N-1} (J(k) - I_r(k))^2,$$

is the mean square error between image  $J$  and the reference image  $I_r$  and  $Q$  is the quantification, worth 255 in our case. The structural similarity index from Wang et al. [12] is defined by

$$MSSIM(J, I_r) = \frac{(2\mu_{I_r}\mu_J + c_1)(2\text{cov}_{J,I_r} + c_2)}{(\mu_{I_r}^2 + \mu_J^2 + c_1)(\sigma_{I_r}^2 + \sigma_J^2 + c_2)},$$

where  $\mu_{I_r}$  (resp.  $\mu_J$ ) is the mean image  $I_r$  (resp.  $J$ ),  $\sigma_{I_r}^2$  its variance and both coefficients are as follows:  $c_1 = 0.01^2$  and  $c_2 = 0.03^2$ .

In each experiment the enhancement parameter  $\epsilon$  was set to 40. This coefficient is deliberately high to better discriminate the possible trends of the results. These two metrics were calculated between an undistorted and unsaturated reference image  $I_R$  (the dynamic is in  $[0, 255]$ ) and unsaturated images obtained after filtering (dynamics can thus be outside the  $[0, 255]$  range). In the images displayed in the following figures the values out of the  $[0, 255]$  range are clipped to 0 or 255.

### 6.1 Experiment 1

Only the first ten frames of each sequence of dataset A were used, with a window size of  $M = 10$ . The results are presented in Table 1 and Figure 5 – in this illustration, only the pictures at 5 meters

are shown as they are more degraded by turbulence than images at 10 meters. This experiment, applied to sequences which can be considered short exposure, gives quite varied results: the values of PSNR and MSSIM are best for the SPCA method in four out of the six tests, which concern Lena and the boat. The most important difference being for Lena (10 m). Visually, the SPCA includes deformations and accentuates rebounds, as can be seen with respect to the hat of the Lena image. However the noise seems more penalizing with the Laplacian filter when trying to distinguish the letters of the poem.



Figure 5: Results of experiment 1 applied on sequences at 5m of dataset A with  $M = 10$  and  $\epsilon = 40$ . From top to bottom:  $\mu$  the average of 10 images,  $L$  computed with the Laplacian filter,  $J$  computed with the SPCA filter.

	Boat 5 m	Lena 5 m	Verse 5 m	Boat 10 m	Lena 10 m	Verse 10 m
Dataset A						
PSNR Laplacian	15.89	13.26	14.67	16.61	13.43	15.75
PSNR SPCA	17.08	13.52	13.97	16.68	19.64	14.15
MSSIM Laplacian	0.09	0.11	0.15	0.26	0.21	0.35
MSSIM SPCA	0.14	0.15	0.12	0.28	0.36	0.19

Table 1: PSNR and MSSIM obtained from the first experiment with the A dataset.

## 6.2 Experiment 2

In Experiment 2 we used the sequence B (resp. C) with a window of size  $M = 10$  (resp.  $M = 20$ ). These sequences can be considered as obtained with long exposure times. In both cases, the average of  $\mu$  is theoretically identical since it is the average of 200 images. It is the same for images enhanced by the Laplacian filter. Table 2 contains numerical results while Figure 6 shows the results for turbulence with a dominant blur and Figure 7 for turbulence with dominant deformation. Strictly speaking the results of the Laplacian PSNR and MSSIM should be identical as  $\mu$  is the average of 20 images averaged over 10; and, in the third case, the average of 10 images averaged over 20. The slight numerical differences observed are due to the production protocol of these averaged pictures: they were averaged and saved in PNG format: decimal values have been rounded.

We observe that the Laplacian PSNR is higher than that of SCPA in 4 out of 6 cases but the MSSIM measure is better for the SCPA in 4 out of 6. In the images of Figure 6, where the blur of turbulence is dominant, we find that the Laplacian is visually noisy especially in the case of the poem. In the case where the deformations are more important than the blur (Figure 7), the SCPA induces local phase shifts, more visible for the boat and the poem.

When the tests on B (with  $M = 10$ ) and C ( $M = 20$ ) are compared, the latter gives better numerical results. In 4 out of 6 cases PSNR is higher, and in 5 out of 6 cases the MSSIM measure is better. This can be explained by the fact that the images used for the input of the SCPA, in case B, are averaged over 20; while they are averaged over 10 in case C. The vector  $w_B$  patch calculated from B, remains more blurred than that calculated from C. This indicates that an increase of the exposure time in image acquisition does not necessarily lead to better results and that an intermediate exposure time should be favored, long enough to limit the effects of deformation but no more.

	Boat 5 m	Lena 5 m	Verse 5 m	Boat 10 m	Lena 10 m	Verse 10 m
Dataset B, $M = 10$						
PSNR Laplacian	17.18	13.06	15.28	17.32	13.17	16.17
PSNR SCPA	17.20	12.43	14.58	17.69	15.01	13.79
MSSIM Laplacian	0.20	0.11	0.21	0.39	0.24	0.42
MSSIM SCPA	0.25	0.09	0.25	0.33	0.33	0.03
Dataset C, $M = 20$						
PSNR Laplacian	17.24	13.06	15.28	17.33	13.17	16.17
PSNR SCPA	16.19	12.64	15.05	17.80	14.88	13.98
MSSIM Laplacian	0.20	0.12	0.22	0.40	0.24	0.43
MSSIM SCPA	0.29	0.17	0.33	0.30	0.34	0.10

Table 2: PSNR and MSSIM obtained from the second experiment with the B and C datasets.

## 7 Conclusion

This paper has studied a well known method [7, 8] that proposes to use the PCA to restore image sequences degraded by turbulence. The study led us to develop a variant of the method proposed in [7, 8] named SCPA. The proposed variant applies to image sequences acquired with short as well as long exposure times which is an improvement over [7, 8]. The effectiveness of the variant that has been proposed in this paper is demonstrated on real turbulence degraded image sequences. Comparative tests show that the results are less noisy than the contrast enhancement by Laplacian filtering. However, the observed local irregularities indicate that Li et al.’s method and its extension



Figure 6: Results of experiment 2 applied on sequences at 5m with  $\epsilon = 40$ . From top to bottom :  $\mu$  the average of 200 images,  $L$  computed with the Laplacian filter,  $J$  computed from the SPCA filter with dataset B and  $M = 10$ ,  $J$  computed from the SPCA filter with dataset C and  $M = 20$ .

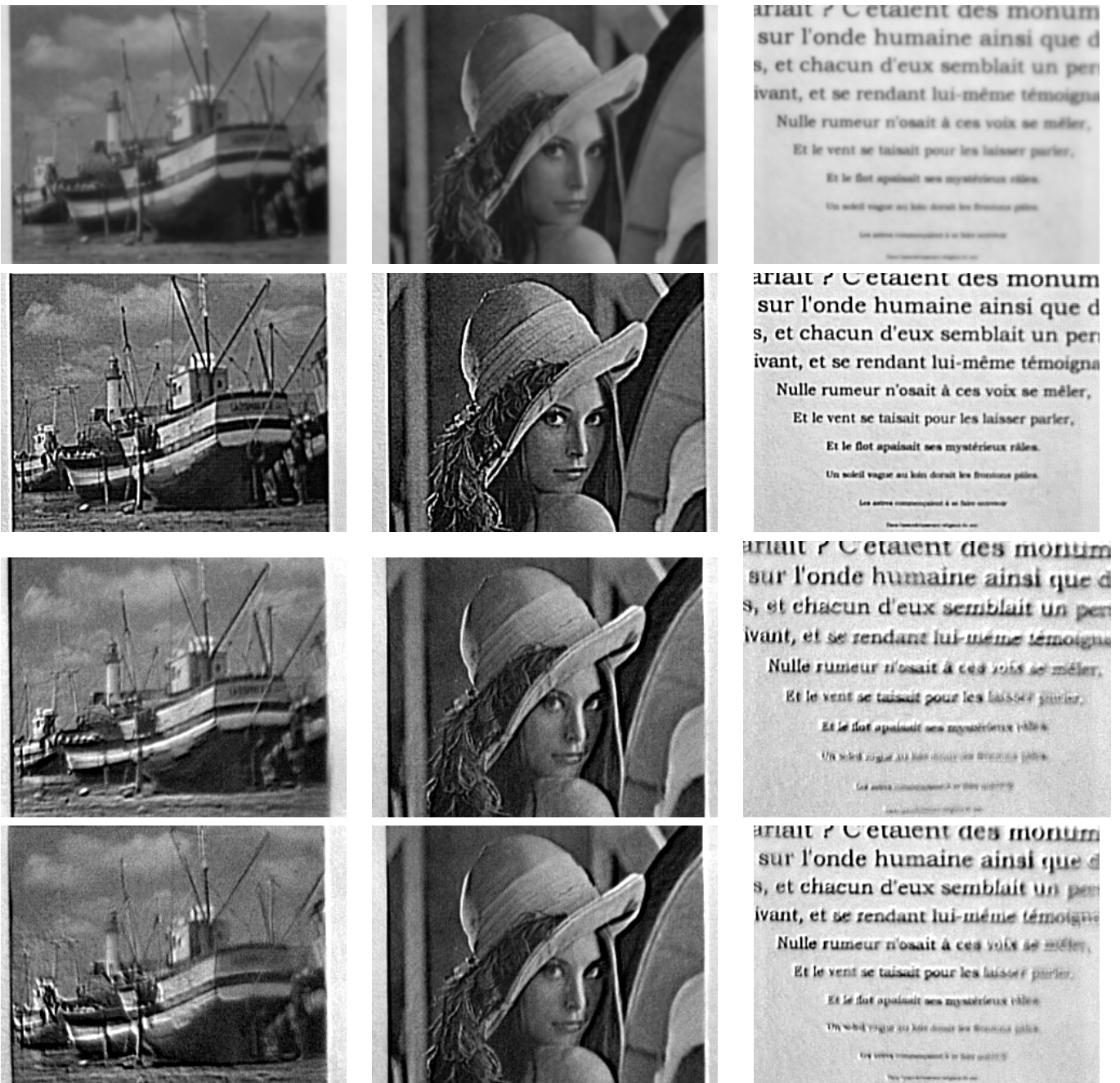


Figure 7: Results of experiment 2 applied on sequences at 10m with  $\epsilon = 40$ . From top to bottom :  $\mu$  the average of 200 images,  $L$  computed with the Laplacian filter,  $J$  computed from the SPCA filter with dataset B and  $M = 10$ ,  $J$  computed from the SPCA filter with dataset C and  $M = 20$ .

the SPCA, should be applied in limited cases of atmospheric turbulence. In addition, a dataset of real atmospheric turbulence degraded sequences has been recorded and is made available for download.

## Acknowledgements

Work partly founded by Centre National d'Études Spatiales (CNES, MISS Project), European Research Council (advanced grant Twelve Labours), Office of Naval research (ONR grant N00014-14-1-0023), Direction Générale de l'Armement, ANR-DGA (project ANR-12-ASTR-0035), FUI (project Plein Phare) and Institut Universitaire de France.

## Credits

All the sequences used in this article are the work of Stéphane Landeau, and available under the CC-BY license. You can use these videos for scientific purpose by citing the article. The poem was composed by Victor Hugo.

## A Acquisition of Image Sequences Seen Through Turbulence

### A.1 Description

Video footage of image sequences through turbulence was done at the Centre de Mathématiques et de Leurs Applications of the École Normale Supérieure Cachan. The experiments consist in filming printed image records. Heat sources were placed on the light path between the printed images and the camera. The camera was mounted on a telescope and placed at a distance of 10 m from the printed image records as depicted in Figure 8. The narrow line of sight of the telescope permitted us to avoid the use of very large heat sources.

Turbulence was created by placing three heat sources along the optical path between the telescope and the printed images. The turbulence zone thus obtained is approximately 1.20 m long. These three heating elements allowed us to maintain a uniform and constant temperature of approximately 240°C at their surface and to stabilize the intensity of the turbulence during the whole experiment.

We obtained several image sequences varying the printed image, the position of the heat sources and the exposure time of the image frames.

Note that in order to record images with a very short time exposure (1 ms), each print is strongly illuminated with halogen lamps (neon lamps are unsuitable because they produce scintillations). The duration of each sequence is 15 s with an acquisition frequency of 13 Hz.

The equipments details are given in Section A.3 and the produced dataset is described in Section A.4.

### A.2 Acquisition

Once the telescope has been focused on each print at a distance of 10 m without turbulence, three video sequences are filmed for each print:

- a reference sequence without turbulence;

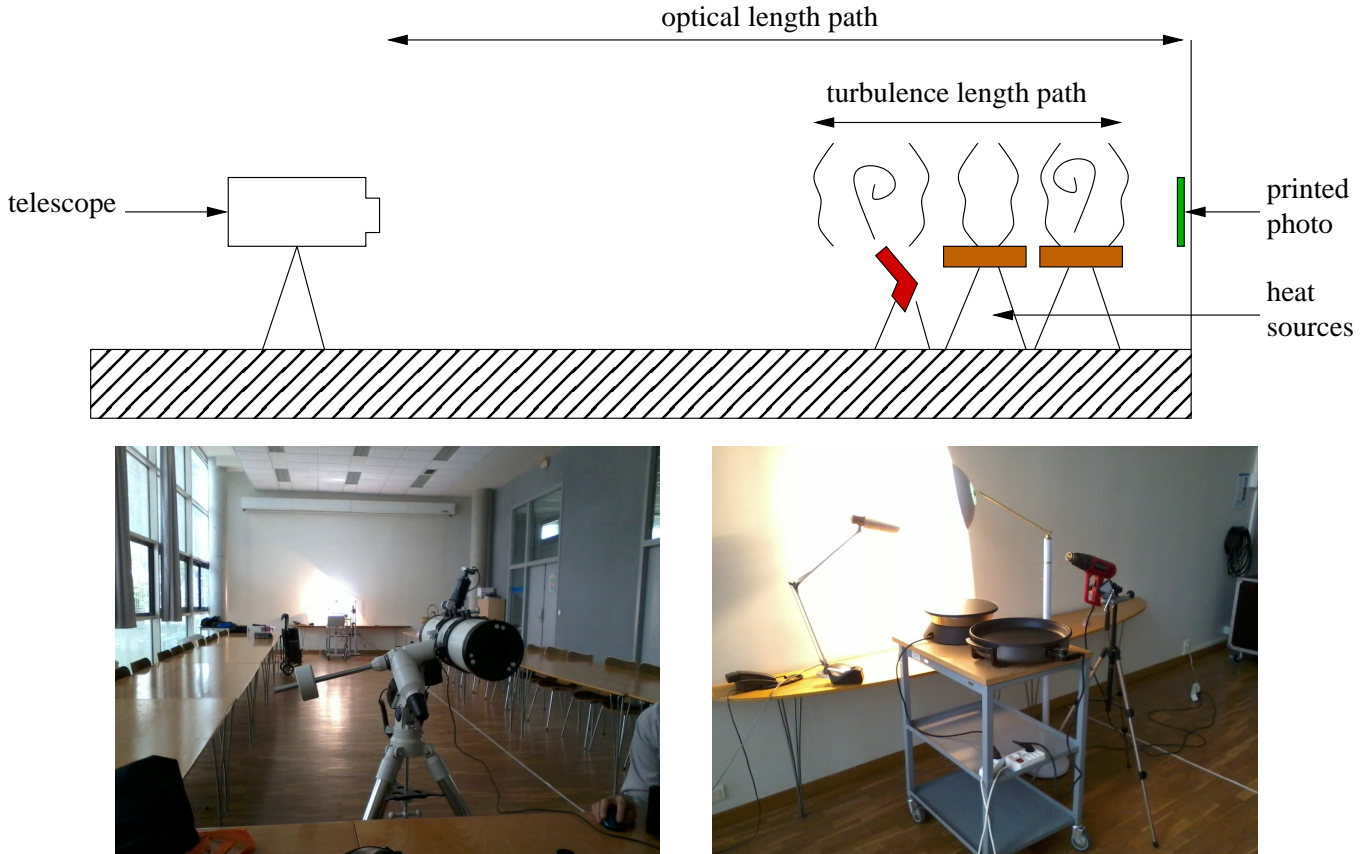


Figure 8: Device and acquisition protocol

- a sequence for which the heat source is placed close to the print, i.e. between 8.80 m and 10.0 m from the telescope;
- a sequence for which the heat source is placed midway between the telescope and the print, i.e. between 4.40 m and 5.60 m from the telescope;

Videos are recorded in AVI format, then frames are extracted in PNG 8-bit format without dynamic stretching between  $[0, 255]$  using the software tool `convert`. To attenuate flicker, each sequence has been stretched to reach the boundaries 0 and 255, by an affine contrast change using its absolute minimum and maximum values.

### A.3 Equipment details

The telescope is a LXD75 6" Newton with a focal length of 762 mm and an aperture of  $f/5$ . The field of view is  $0.27^\circ$  (H)  $\times$   $0.20^\circ$  (V) and covers a surface of  $4.70 \text{ cm} \times 3.53 \text{ cm}$  at 10 m. At the focal point is placed the CCD module of a Philips spc900nc webcam equipped with a Sony ICX098  $1/4''$  CCD sensor. The acquisition image format is set to  $320 \times 240$  with a progressive scan.

### A.4 Dataset description

The image sequence dataset is available both in AVI format and coded in PNG 8-bit grayscale format with a size of  $320 \times 240$ . There are four kinds of sequences: the classical Lena, the classical boat "La Cornouaille", a mire of black round points, and a typeset verse with different font sizes, as listed

below. We varied the exposure time so that the blur (long exposure time) or the deformations (short exposure time) dominate.

video name	images name	number of images	blur/deformation	comment
lena_05m_a.avi	lena_05m_a-xxx.png	200	dominant/weak	
lena_10m_a.avi	lena_10m_a-xxx.png	200	weak/dominant	
lena_10m_R.avi	lena_R-xxx.png	200	no	reference
bateau_05m_a.avi	bateau_05m_a-xxx.png	200	dominant/weak	
bateau_10m_a.avi	bateau_10m_a-xxx.png	200	weak/dominant	
bateau_10m_R.avi	bateau_R-xxx.png	200	no	reference
points_05m_a.avi	points_05m_a-xxx.png	200	dominant/weak	
points_10m_a.avi	points_10m_a-xxx.png	200	weak/dominant	
points_10m_R.avi	points_R-xxx.png	200	no	reference
poeme_05m_a.avi	poeme_05m_a-xxx.png	200	dominant/weak	
poeme_10m_a.avi	poeme_10m_a-xxx.png	200	weak/dominant	
poeme_10m_R.avi	poeme_R-xxx.png	200	no	reference

## B Practical computation of the eigenvectors

This section gives the proof that in order to compute the eigenvectors of  $\Sigma$  it suffices to calculate the eigenvectors  $v_i$  of the much smaller matrix  $A^T A \in \mathcal{M}_{M \times M}(\mathbb{R})$  where  $M \ll N$ .

For any eigenvector  $v_i \in \mathbb{R}^M$  of  $A^T A \in \mathcal{M}_{M \times M}(\mathbb{R})$  we have  $A^T A v_i = \lambda_i v_i$  for some eigenvalue  $\lambda_i$ . Therefore, by multiplying the above equation on the left by  $A$  we have  $AA^T(Av_i) = \lambda_i(Av_i)$ . Hence, we deduce that  $Av_i$  is an eigenvector (with eigenvalue  $M\lambda_i$ ) of  $\Sigma$ . This means that the computation of any eigenvector of  $A^T A$  provides an eigenvector of  $\Sigma$ . It remains to show that by computing the eigenvectors of  $A^T A$  we obtain, in fact, *all* the eigenvectors of  $\Sigma$ . Since  $\text{rank}(A^T A) = \text{rank}(AA^T)$  we deduce that  $\text{rank}(A^T A) = \text{rank}(\Sigma)$ . Therefore, the number of eigenvectors of  $A^T A$  equals the number of eigenvectors of  $\Sigma$ . Consequently, to compute *all* the eigenvectors of  $\Sigma \in \mathcal{M}_{N \times N}(\mathbb{R})$ , it suffices to calculate *all* the eigenvectors of  $A^T A \in \mathcal{M}_{M \times M}(\mathbb{R})$ .

## C Online demonstrator setup

The online demonstrator presents an extension of the SPCA algorithm in the sense that we consider a temporal sliding window of length  $M$  applied on an input sequence of images  $(I_t)_{1 \leq t \leq T}$  of duration  $T, T \geq M$ . The SPCA is applied for  $t = 1, \dots, T - M$  to the sequence  $(I_m)_{t \leq m \leq t+M}$  so that Equations (3), (5) and (8) are respectively rewritten with the  $t$  index

$$\mu_t = \frac{1}{M} \sum_{m=t}^{t+M} I_m, \quad (9)$$

$$J_t = \mu_t - \epsilon \frac{\langle \Delta \mu_t, w_t^i \rangle}{|\langle \Delta \mu_t, w_t^i \rangle|} w_t^i, \quad (10)$$

$$L_t = \mu_t - \epsilon \frac{\Delta \mu_t}{\|\Delta \mu_t\|}. \quad (11)$$

The demonstrator shows for each time  $t$  (up to  $t = 9$ ) the different filtered frames and components. Image  $w_t^b$  corresponds to the selected image vector among  $w_t^1$  and  $w_t^2$  (see Figure 9). External input

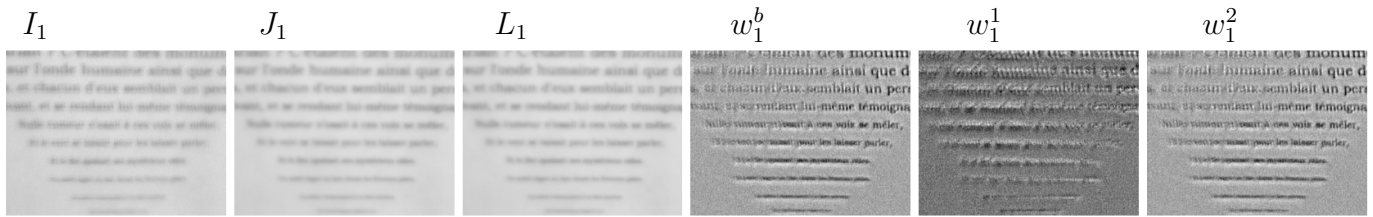


Figure 9: Example of frames shown in the demonstrator corresponding to the “verse 5m” sequence at time  $t = 1$  for a sliding window of length  $M = 10$  and  $\epsilon = 0.5$ .

sequences must be provided to the demonstrator as a TAR archive containing the frames. The TAR file must not have been compressed.

## References

- [1] J.M. BECKERS, *Adaptive optics for astronomy: Principles, performance, and applications*, Annual Review of Astronomy and Astrophysics, 31 (1993), pp. 13–62. <https://doi.org/10.1146/annurev.aa.31.090193.000305>.
- [2] D.L. FRIED, *Optical resolution through a randomly inhomogeneous medium for very long and very short exposures*, Journal of the Optical Society of America, 56 (1966), pp. 1372–1379. <https://doi.org/10.1364/JOSA.56.001372>.
- [3] —, *Probability of getting a lucky short-exposure image through turbulence*, Journal of the Optical Society of America, 68 (1978), pp. 1651–1658. <https://doi.org/10.1364/JOSA.68.001651>.
- [4] R. E. HUFNAGEL AND N. R. STANLEY, *Modulation transfer function associated with image transmission through turbulent media*, Journal of the Optical Society of America, 54 (1964), pp. 52–61. <https://doi.org/10.1364/JOSA.54.000052>.
- [5] A.N. KOLMOGOROV, *The local structure of turbulence in incompressible viscous fluid for very large Reynolds numbers*, Doklady Akademiia Nauk SSSR, 30 (1941), pp. 301–305.
- [6] L. LEBART, A. MORINEAU, AND M. PIRON, *Statistique exploratoire multidimensionnelle*, Dunod, 3 ed., 2000, ch. 1. ISBN 2100053515.
- [7] D. LI, R.M. MERSEREAU, AND S. SIMSKE, *Atmospheric turbulence-degraded image restoration using principal components analysis*, IEEE Letters on Geoscience and Remote Sensing, 4 (2007), pp. 340–344. <http://dx.doi.org/10.1109/LGRS.2007.895691>.
- [8] D. LI, S. SIMSKE, AND R.M. MERSEREAU, *Blind image deconvolution using constrained variance maximization*, in Proceedings of the IEEE Conference on Signals, Systems and Computers, vol. 2, 2004, pp. 1762–1765. <http://dx.doi.org/10.1109/ACSSC.2004.1399463>.
- [9] K. LIU, Q. DU, H. YANG, AND B. MA, *Optical flow and principal component analysis-based motion detection in outdoor videos*, EURASIP Journal on Advances in Signal Processing, (2010), pp. 1–1. <http://dx.doi.org/10.1155/2010/680623>.
- [10] V.I. TATARSKI, *Wave propagation in a turbulent medium*, Science, 134 (1961), pp. 324–325. Translated from Russian by R. A. Silverman.

- [11] M. TURK AND A. PENTLAND, *Eigenfaces for recognition*, Journal of Cognitive Neuroscience, 3 (1991), pp. 71–86. <http://dx.doi.org/10.1162/jocn.1991.3.1.71>.
- [12] ZHOU W., A.C. BOVIK, H.R. SHEIKH, AND E.P. SIMONCELLI, *Image quality assessment: from error visibility to structural similarity*, IEEE Transactions on Image Processing, 13 (2004), pp. 600–612. <https://doi.org/10.1109/TIP.2003.819861>.